Atomic layer etching of Sn by surface modification with H and Cl radicals

IOP Publishing Nanotechnology
Nanotechnology 34 (2023) 035301 (9pp) https://doi.org/10.1088/1361-6528/ac9981

Atomic layer etching of Sn by surface modification with H and Cl radicals

Doo San Kim[1], Yun Jong Jang[1], Ye Eun Kim[1], Hong Seong Gil[1], Byeong Hwa Jeong[1,2] and Geun Young Yeom[1,3]

[1] School of Advanced Materials Science and Engineering, Sungkyunkwan University, Suwon 16419, Republic of Korea
[2] Korea Institute for Super Materials, ULVAC KOREA, Pyeongtaek 17792, Republic of Korea
[3] SKKU Advanced Institute of Nano Technology (SAINT), Sungkyunkwan University, Suwon 16419, Republic of Korea

E-mail: gyyeom@skku.edu

Received 10 July 2022, revised 26 September 2022
Accepted for publication 12 October 2022
Published 4 November 2022

Abstract

Sn is the one of the materials that can be used for next generation extreme ultraviolet (EUV) mask material having a high absorption coefficient and, for the fabrication of the next generation EUV mask, a precise etching of Sn is required. In this study, the atomic layer etching (ALE) process was performed for the precise etch thickness control and low damage etching of Sn by the formation SnH_xCl_y compounds on the Sn surface using with H and Cl radicals during the adsorption step and by the removal of the compound using Ar^+ ions with a controlled energy during the desorption step. Through this process, optimized ALE conditions with different H/Cl radical combinations that can etch Sn at ~2.6 Å $cycle^{-1}$ were identified with a high etch selectivity over Ru which can be used as the capping layer of the EUV mask. In addition, it was confirmed that not only the Sn but also Ru showed almost no physical and chemical damage during the Sn ALE process.

Supplementary material for this article is available online

Keywords: atomic layer etching (ALE), tin (Sn), ruthenium (Ru), absorber layer, capping layer, high selectivity

(Some figures may appear in colour only in the online journal)

1. Introduction

The degree of integration of semiconductor devices is continuously increasing, and the minimum line width of the pattern has also decreased to 10 nm or less. To realize this, the light source used in the photolithography process has been replaced from argon fluoride (ArF, 193 nm) to extreme ultraviolet (EUV, 13.5 nm), and, as the wavelength of the light source is very short, the photomask has been also changed from the existing transmission type mask to the reflection type mask [1–5]. The reflective mask for EUV lithography consists of a multilayer reflective film that reflects the light, a capping layer preventing oxidation and contamination of the reflective film, and an absorbing layer that absorbs EUV light to form a pattern. In general, a multi-layer of Mo/Si is used for the multi-layer reflective film, Ru for the capping layer, and Ta, TaN, TaBN, etc are used as the EUV absorbing layer [6–11]. In the reflective mask, a thin absorbing layer is required due to the shadowing effect. However, in the case of Ta-based materials, it is difficult to lower the thickness because of the decrease in the degree of EUV blocking, and which affects the patterning [12, 13]. In addition, it is necessary to have a high etch selectivity with the capping layer in the process of pattern formation for the EUV absorption layer and to minimize etch damage such as a change in surface roughness [14, 15]. Therefore, as the next generation EUV absorber layer, not only the materials with a higher extinction coefficient than Ta but also a precise etching control of the materials is required.

Several studies on the etching of EUV mask materials can be found in the literature. For example, plasma etching techniques for Ta-based materials using Cl_2 have been

investigated [16–19], but it is difficult to apply for the next generation EUV mask fabrication not only due to the limitation of the extinction coefficient but also due to the lack of precise etch control. Etching study on Cr has been reported [20], and for the etching of Cr, a precise etching control was performed using ion milling or atomic layer etching (ALE), but Cr also has a low extinction coefficient for the next generation EUV absorber. Recently, a research on the etching of Ni, a material with a higher extinction coefficient than Ta-based materials, has been investigated through a plasma-thermal ALE method, and a precisely control of Ni etching and anisotropic etching by repeating oxidation and a ligand exchange have been reported [21, 22]. However, there are no sufficient studies on the etching of EUV materials with high absorption coefficients applicable to the next generation EUV mask such as precise etching characteristics, the evaluation of etch selectivity with the capping layer, the degree of damage to the capping layer during the etch process, etc.

In this study, anisotropic ALE studies were conducted on tin (Sn), which is one of the materials with a high absorption coefficient applicable to next generation EUV mask, by modifying the Sn surface with reactive radicals and by removing the modified surface layer by ion bombardment. Cl_2/H_2 plasmas were used to modify the Sn surface to form a compound layer such as SnH_x, $SnCl_x$, SnH_xCl_y, etc on the Sn surface. Thereafter, the modified Sn surface layer was removed using Ar^+ ions with a controlled energy. Through this cyclic process, a possibility of a self-limited precise Sn etching with a high etch selectivity and a low surface damage to the Ru capping layer was investigated.

2. Experimental

The ALE system used in the experiment is shown in figure 1(a). A cylindrical type inductively coupled plasma (ICP) source operated with a 13.56 MHz radio-frequency (RF) generator was located at the upper part of the chamber. Reaction gases such as H_2, Cl_2, and Ar were injected through the gas inlet holes at the lower part of the ICP source. A three-grid assembly made of graphite was installed under the ICP source to extract and accelerate the ions generated in the plasma. A positive voltage was applied to the 1st grid for the Ar^+ ion energy control and a negative voltage to the 2nd grid to form a parallel beam and to control the ion flux while grounding the 3rd grid. Between the ion source and the substrate, a shutter was located to block the ions and to adsorb H/Cl radicals on the substrate during the reactive gas adsorption step and, during the desorption step, the shutter was removed to expose the substrate with energetic Ar^+ ions. The substrate was maintained at 20 °C through a chiller. In addition, before the process, the base pressure of the chamber was maintained at less than 2×10^{-6} Torr through a turbo molecular pump.

For Sn ALE experiment, 100 nm thick Sn was deposited by sputtering on a Si substrate with a titanium (Ti) layer and a photoresist (PR) pattern was formed on the Sn layer through a photolithography process for the etch depth measurement. The Sn ALE concept is shown in figure 1(b). During the adsorption step, H and Cl radicals are extracted from the ICP source using H_2/Cl_2 plasmas, and then adsorbed on the Sn surface to form SnH_xCl_y. In order to modulate the ratio of H and Cl in the process of forming SnH_xCl_y on the Sn surface, the ratio of H_2/Cl_2 gas flow rates to the plasma was varied. As the adsorption conditions, 3 mTorr of H_2/Cl_2 gas pressure was maintained, and 300 W of 13.56 MHz RF power was applied to the ICP source and, only radicals were exposed to the substrate by closing the shutter to block the ions reaching the substrate while applying no voltages to the grid assembly. As the desorption condition, 3 mTorr of Ar pressure was maintained and 300 W of 13.56 MHz RF power was also applied to form an Ar plasma. Then, $0 \sim +80$ V was applied to the 1st grid and -250 V was applied to the 2nd grid to extract the Ar^+ ion beam to the substrate while grounding the 3rd grid, and the shutter was opened to etch the substrate. The gas remaining in the chamber was removed through a purge step between each adsorption and desorption step, and the ALE process was performed by configuring one cycle of adsorption-purge-desorption-purge.

In order to measure the etch thickness of Sn, the Sn ALE process was performed for 100 cycles, and after removing the PR, the etch per cycle (EPC) was measured using a surface profilometer (Tencor Instrument, Alpha step 500). To measure the ion energy of the Ar^+ ion beam used for etching, a retarding grid ion energy analyzer was installed on the substrate and the ion energy distribution according to the 1st grid voltage was measured. Also, optical emission spectroscopy (OES; Avantes, AvaSpec-3648) was performed to observe the changes in the radical species in the plasmas. The surface composition and its binding status during the Sn ALE process were measured by x-ray photoelectron spectroscopy (XPS; Thermo VG, MultiLab 2000, Al Kα source) and the surface roughness was measured by atomic force microscope (AFM; PSIA, XE 100) to investigate the physical damage. In addition, secondary ion mass spectrometry (SIMS; ION-TOF, TOF-SIMS-5) was used to determine the depth of H adsorbed on the Sn surface during the adsorption with H_2/Cl_2 plasma in the ALE process.

3. Results and discussion

An ALE process cycle is composed of an adsorption step and a desorption step and, to configure the Ar^+ ion energy range required for the desorption step, the effect of Ar^+ ion energy on the sputter etch depth/cycle of Sn was investigated and the result is shown in figure 2(a). The 1st grid voltage was varied from 0 to +80 V while maintaining the 2nd grid voltage at –250 V. The ICP source was operated at 3 mTorr Ar and 300 W of RF power. The etch cycle was consisted of 30 s of desorption/10 s of purge and the etching was processed to 100 cycles for the calculation of the EPC. As shown in figure 2(a), the EPC was 0 up to +50 V of 1st grid voltage and, ~0.6 and ~1.8 Å cycle^{-1} were observed for 60 and 80 V of 1st grid voltages, respectively. Therefore, not to sputter etch Sn, up to +50 V of 1st grid voltage can be used for the

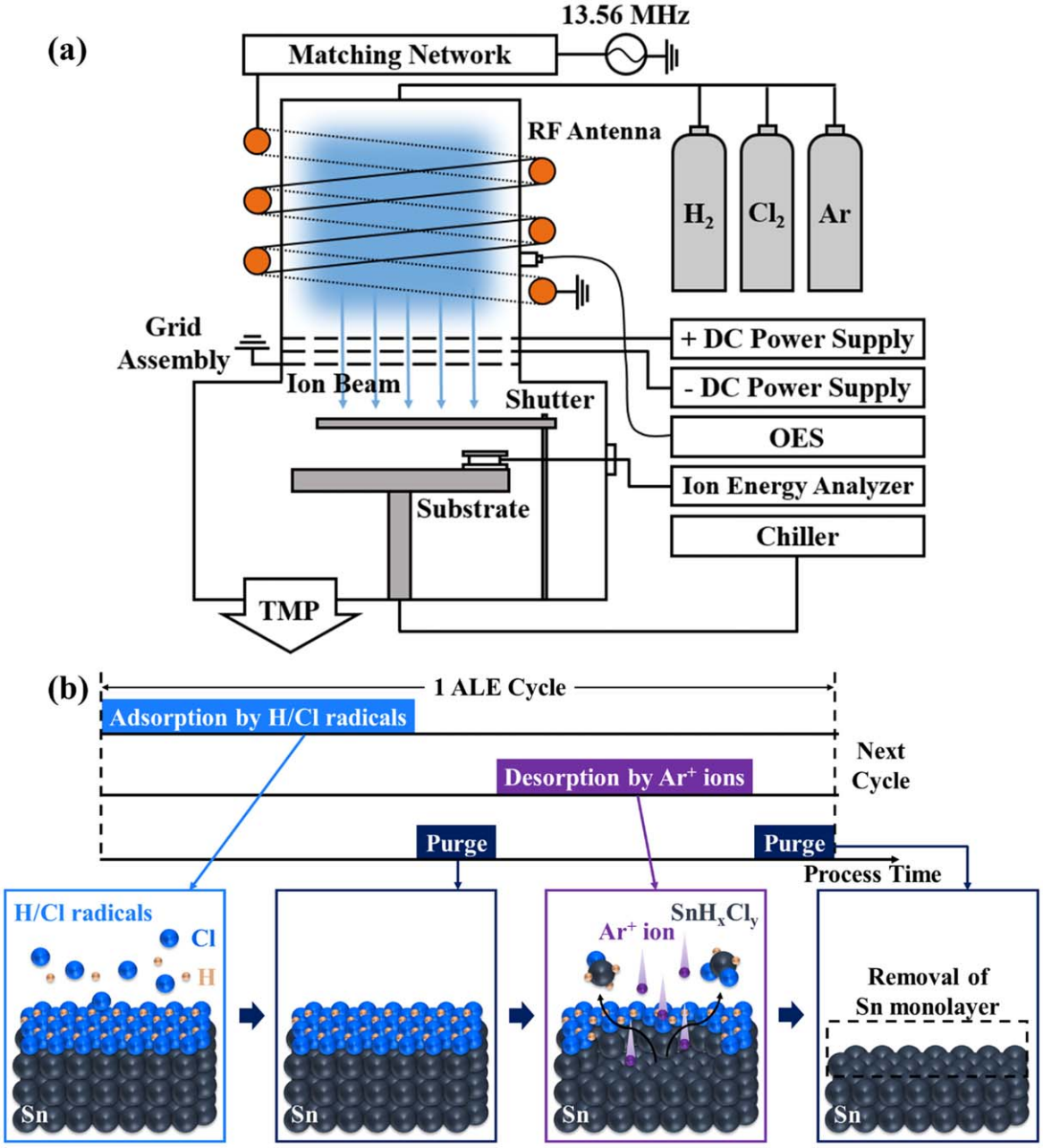

Figure 1. (a) Schematic diagram of ICP type ion beam system used for ALE of Sn. (b) The ALE concept for Sn etching by adsorption of H/Cl radicals and desorption of Ar^+ ions.

ion energy of Sn ALE during the desorption step. The inset figure in figure 2(a) shows the Ar^+ ion energy distribution measured for different 1st grid voltage and, the actual Ar^+ ion energy was 10–20 eV higher than the 1st grid voltage possibly due to the plasma potential developed in the ICP source (The ion current in the substrate for the Ar^+ ion beam is shown in figure S1 of the supplementary.). Therefore, it is believed that the threshold energy for noticeable Sn sputtering by Ar^+ ion in our experiments is ~65 eV (in fact, actual Sn sputter threshold energy can be much lower than +65 eV if unnoticeably small sputtering yield/ion is considered.) Therefore, by using +50 V of 1st grid voltage, the Sn ALE processes were performed with/without the adsorption of Cl radicals during the adsorption step. Figure 2(b) shows the EPC measured as a function of the desorption time from 0 to 40 s by Ar^+ ions during the desorption step with the +50 V of 1st grid voltage with/without the adsorption of Cl radicals during the adsorption step. For the adsorption of Cl radicals, 3 mTorr Cl_2 and 300 W of 13.56 MHz RF power were used for ICP source with the shutter-on to remove possible ion bombardment and the Sn surface was exposed to Cl radicals for 30 s. As shown in figure 2(b), when Cl radicals were not adsorbed, no etching of Sn was observed for the desorption time from 0 to 40 s indicating no sputter etching of Sn (black square dots). Even though Cl radicals were adsorbed, no Sn etching was also observed when the desorption time by Ar^+ ions was 0 s indicating no spontaneous etching of Sn by Cl radical adsorption only. However, with increasing the Ar^+ ion

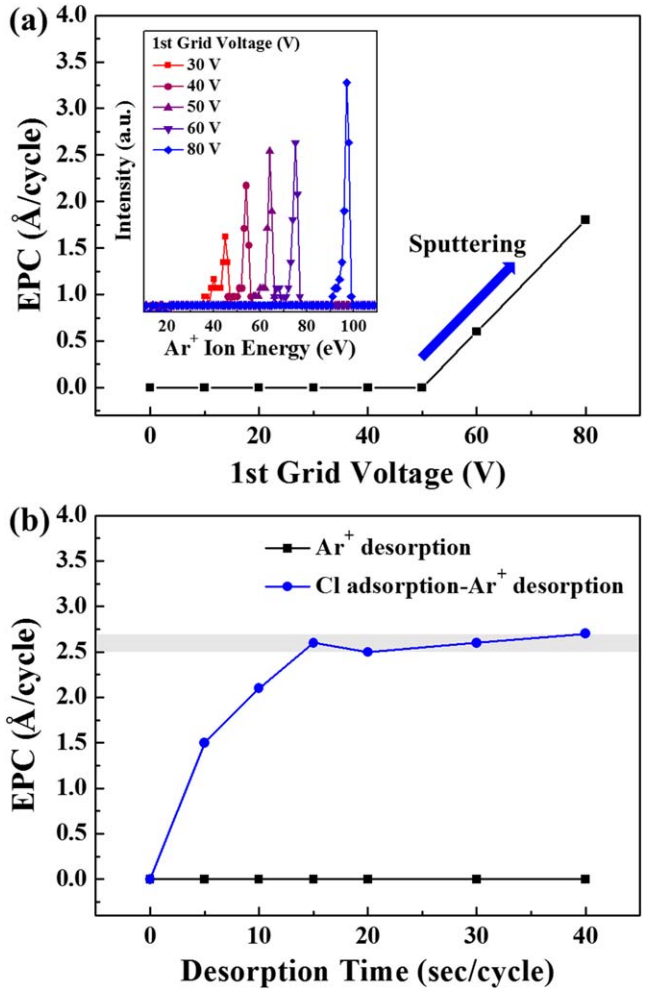

Figure 2. (a) Effect of Ar^+ ion energy on the sputter etch depth/cycle (EPC) of Sn without adsorption of H/Cl radicals, therefore, the EPC just by sputtering with Ar^+ ions (one cycle = 30 s of Ar^+ ion sputtering and 10 s of purging). (b) EPC measured as a function of the desorption time from 0 to 40 s by Ar^+ ions during the desorption step with +50 V of 1st grid voltage with/without the adsorption of Cl radicals during the adsorption step. Inset figure in (a) shows the Ar^+ ion energy distribution measured for different 1st grid voltages. For (a), the ICP source was operated at 3 mTorr Ar and 300 W of 13.56 MHz RF power. For the adsorption of Cl radicals, 3 mTorr Cl_2 and 300 W of 13.56 MHz RF power were used with the shutter-on to remove possible ion bombardment and the Sn surface was exposed to Cl radicals for 30 s.

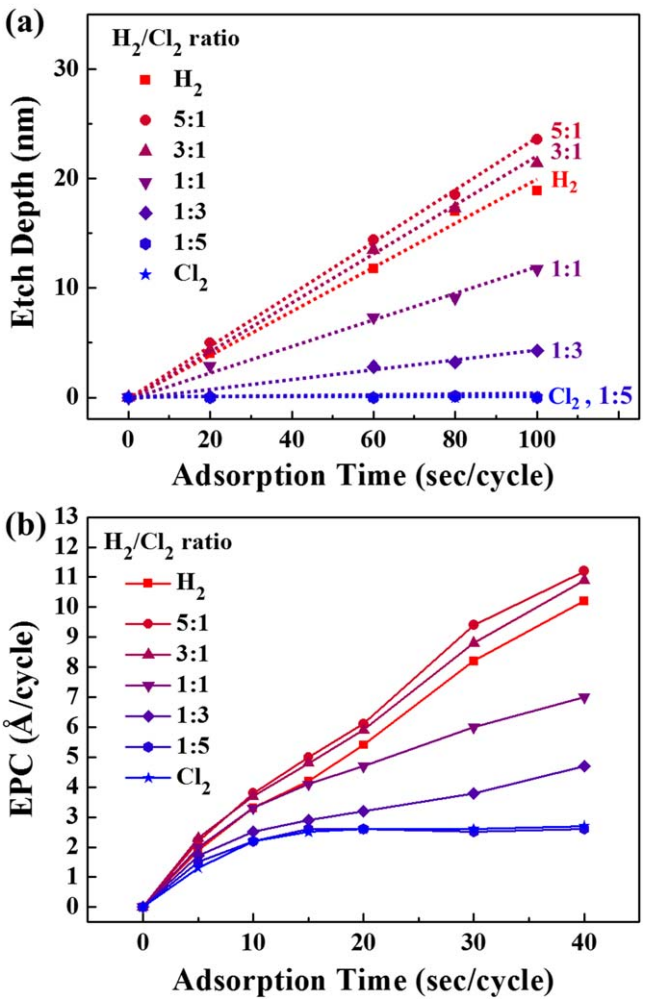

Figure 3. (a) EPC of Sn measured as a function of H_2/Cl_2 gas ratios in the ICP source during the adsorption step. The EPC cycle was consisted of the H/Cl adsorption for 30 s and purge for 10 s without the desorption step. (b) EPC of Sn measured as a function of adsorption time for different gas ratios of H_2/Cl_2 during the adsorption step with the desorption step. The adsorption conditions were the same as those in (a) and, for the desorption, +50 V to the 1st was applied for 15 s while operating the ICP source with Ar 3 mTorr and 300 W of RF power.

Table 1. Boiling points of the Sn hydride and Sn chloride.

Name	Formula	Boiling point (°C)
Stannane	SnH_4	−52
Chlorostannane	SnH_3Cl	33.7
Dichlorostannane	SnH_2Cl_2	59
Trichlorostannane	$SnHCl_3$	89
Tin Chloride	$SnCl_4$	114

desorption time after the Cl radical adsorption, the EPC was increased gradually and finally reached at saturated EPC of ~2.6 Å after 15 s of desorption time. The saturation of EPC after 15 s of desorption time is related to the removal of all of the Cl radical adsorbed Sn on the Sn surface and the exposure of bare Sn surface. From the figure 2, the desorption condition for the Sn ALE was identified as the +50 V of 1st grid voltage and 15 s of desorption time.

To investigate the adsorption condition for the Sn ALE, the Sn surface was adsorbed with H/Cl radicals without the desorption step. Figure 3(a) shows the EPC measured as a function of gas ratio of H_2/Cl_2 for the adsorption gas in the ICP source during the adsorption step. The EPC cycle was consisted of H/Cl adsorption for 30 s and purge for 10 s without the desorption step. The ICP source was also operated at 3 mTorr and 300 W of RF power without applying voltages to grid assembly and with the shutter-on. The EPC was calculated after running 100 cycles. As shown in figure 3(a), when the ratio of H_2/Cl_2 in the adsorption gas mixture was 1/5 or 0/1, therefore, when the gas mixture was a highly chlorine rich gas, no etching of Sn was observed up to 100 s

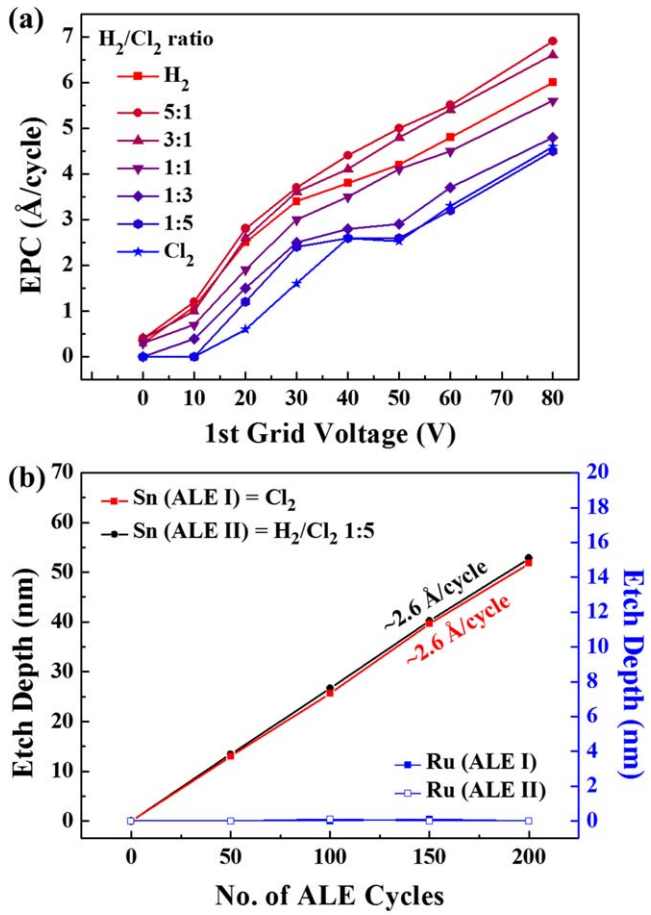

Figure 4. (a) Effect of Ar^+ ion energy (1st grid voltage) on EPC for different gas ratios of H_2/Cl_2. (b) Etch depths of Sn and Ru measured as a function of the number of etch cycles with the two optimized Sn ALE processes (ALE I = adsorption by Cl_2 for 15 s, desorption by +40 V for 15 s, ALE II = adsorption by H_2/Cl_2 of 1/5 for 15 s, desorption by +30 V for 15 s).

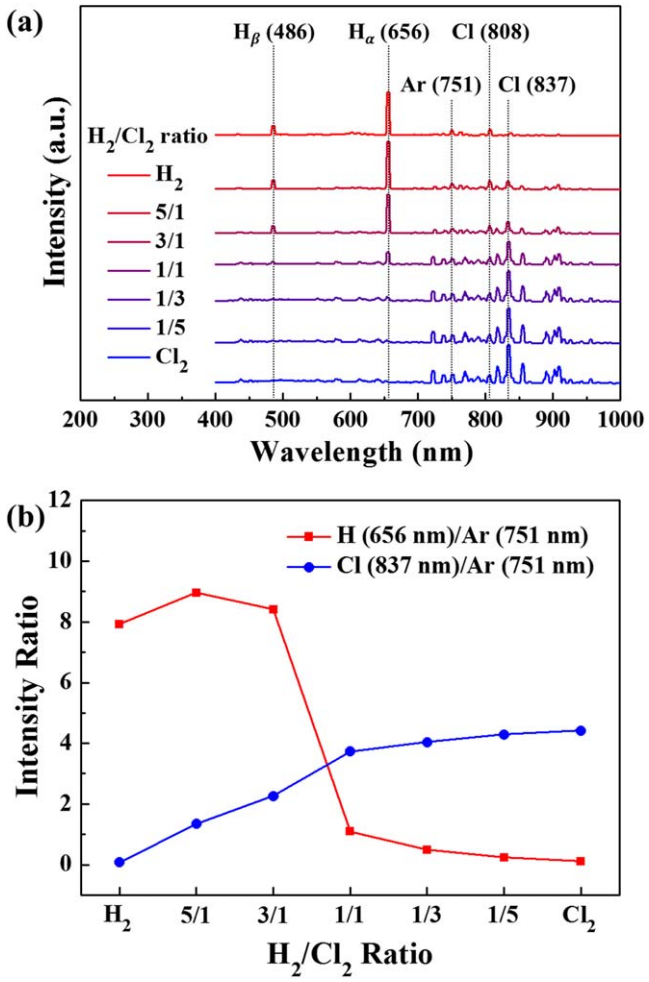

Figure 5. (a) OES spectra for different H_2/Cl_2 gas ratios in the ICP source. For the comparison of H and Cl radicals, 0.3 mTorr of Ar was added in the 3 mTorr of H_2/Cl_2 plasmas. (b) The ratios of H(656 nm)/Ar(751 nm) and Cl(837 nm)/Ar(751 nm) in (a) measured for different gas ratios of H_2/Cl_2 for the rough estimation of H and Cl radicals in the plasmas.

of adsorption time. However, as the ratio of H_2 is increased in the H_2/Cl_2 adsorption gas mixture, the increase of EPC with the increase of adsorption time was observed indicating spontaneous etching of Sn during the adsorption step (it has already been reported that Sn reacts with H radical and is etched spontaneously in H and H-rich gas environments [10, 23, 24]). The EPCs for the H_2/Cl_2 gas ratios of 3/1 and 5/1 were slightly higher than that for H_2 only. Therefore, it is found that, for the adsorption condition with H_2/Cl_2 gas mixtures, a H_2/Cl_2 gas mixture of lower than 1/5 or pure Cl_2 is required to prevent spontaneous etching during the adsorption step. Table 1 shows the boiling points of Sn chlorides and Sn hydrides. The boiling point of $SnCl_4$ is 114 °C, the boiling point of SnH_4 (stannane) is −52 °C, and the boiling points of SnH_xCl_y are 33.7 (SnH_3Cl), 59 (SnH_2Cl_2), and 89 °C ($SnHCl_3$). Therefore, with increasing H_2 in the H_2/Cl_2 gas mixture during the adsorption step, the SnH_xCl_y compounds having lower boiling points are formed on the Sn surface, and spontaneous etching is increased.

Figure 3(b) shows the Sn EPC measured as a function of adsorption time for different gas ratios of H_2/Cl_2 during the adsorption step with the desorption step. The adsorption conditions were the same as those in figure 3(a) and, for the desorption, +50 V to the 1st grid and −250 V to the 2nd grid were applied for 15 s while operating the ICP source with Ar 3 mTorr and 300 W of RF power. As shown in figure 3(b), for the adsorption gas of Cl_2 and 1/5 of H_2/Cl_2, the EPC was initially increased with the increase of adsorption time due to the increased coverage of H/Cl on the Sn surface and the preferential removal of SnH_xCl_y compounds formed on the Sn surface during the desorption step (the bond dissociation energies of Sn-H and Sn-Cl are 2.78 and 4.22 eV, respectively, while that of Sn-Sn is 2.03 eV, therefore, SnH_xCl_y are preferentially removed during the desorption step). When the Sn surface was exposed to H/Cl longer than ~15 s of adsorption time, due to the full coverage of H/Cl on the Sn surface during the adsorption step, the saturation of EPC at ~2.6 Å $cycle^{-1}$ could be observed. When the adsorption gas ratio of H_2/Cl_2 is higher than 1/5, even though the EPC is also initially increased with increased adsorption time, the EPC was higher than those for the H_2/Cl_2 gas ratio of ⩽1/5 by showing 2.9, 4.1, 4.8, 5.0, and 4.2 Å $cycle^{-1}$ at 15 s for

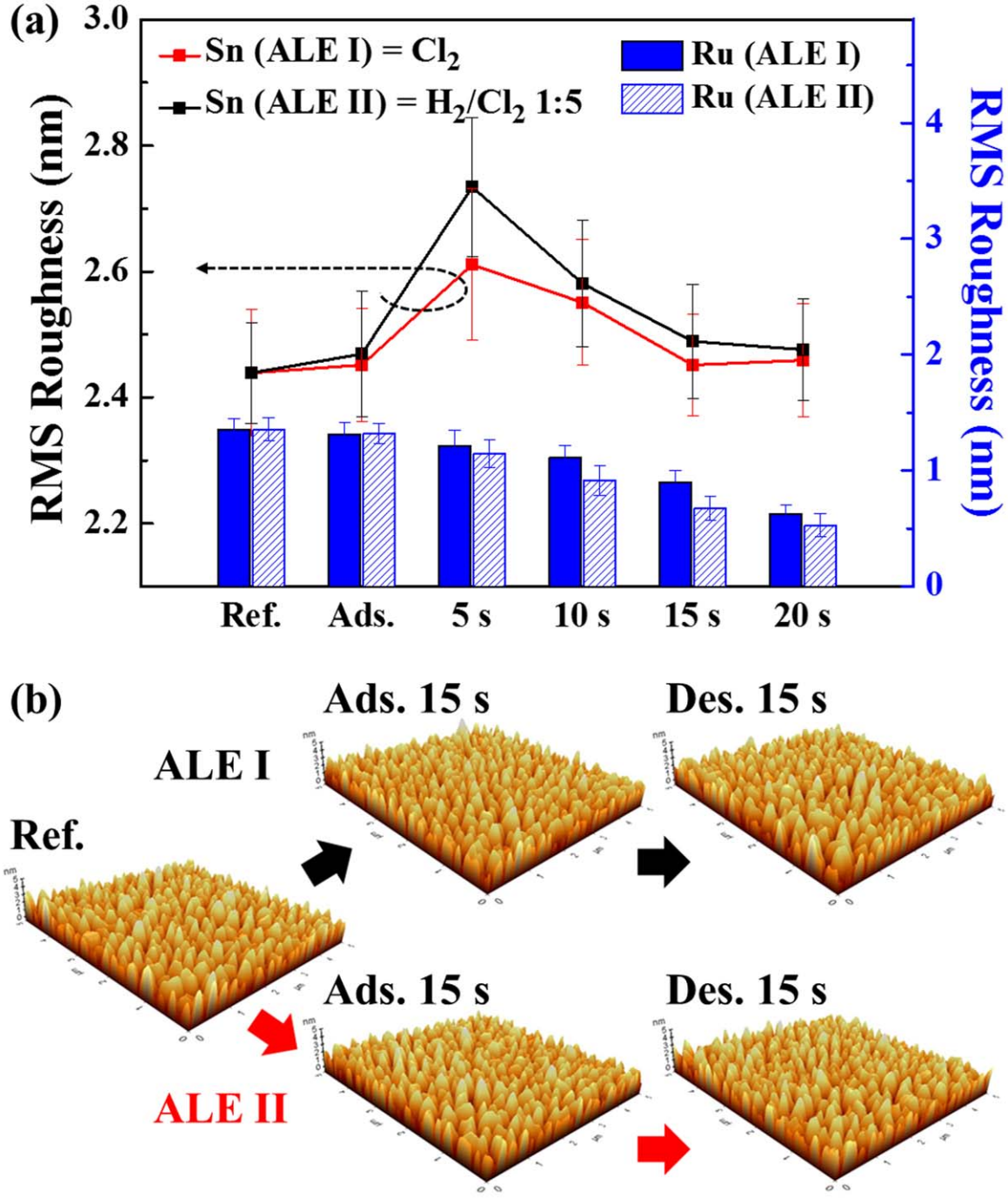

Figure 6. Changes in the RMS surface roughness of Sn investigated by AFM before adsorption (the reference), after the adsorption, and during the desorption for Sn ALEs. (a) RMS surface roughness values of Sn and Ru during the ALEs for the desorption time from 0 to 20 s for the two ALE conditions of ALE I and ALE II shown in figure 4(b). (b) 5 μm × 5 μm 3D AFM images of Sn surface during Sn ALE processes of ALE I and ALE II.

H_2/Cl_2 of 1/3, 1/1, 3/1, 5/1, and 1/0, respectively, and the EPC was not saturated at a higher adsorption time due to the formation of volatile SnH_xCl_y compounds as shown in figure 3(b) and the spontaneous etching of SnH_xCl_y during the adsorption step. Therefore, for the self-limited Sn ALE, H_2/Cl_2 ratio of $\leqslant 1/5$ and $\geqslant 15$ s of adsorption time were required.

While keeping the adsorption time and desorption time at 15 s each, the effect of 1st grid voltage, therefore, the effect of Ar^+ ion energy on the EPC for different gas ratios of H_2/Cl_2 was investigated and the results are shown in figure 4(a). For pure Cl_2, the EPC was increased with the increase of 1st grid voltage due to the partial removal of the SnH_xCl_y modified layer formed on the Sn surface at the lower Ar^+ ion energy and was saturated at +40–50 V of 1st grid voltage at ~2.6 Å by the complete removal of the SnH_xCl_y. And, the further increase of 1st grid voltage increased the EPC due to the sputtering of Sn exposed after the removal of the SnH_xCl_y

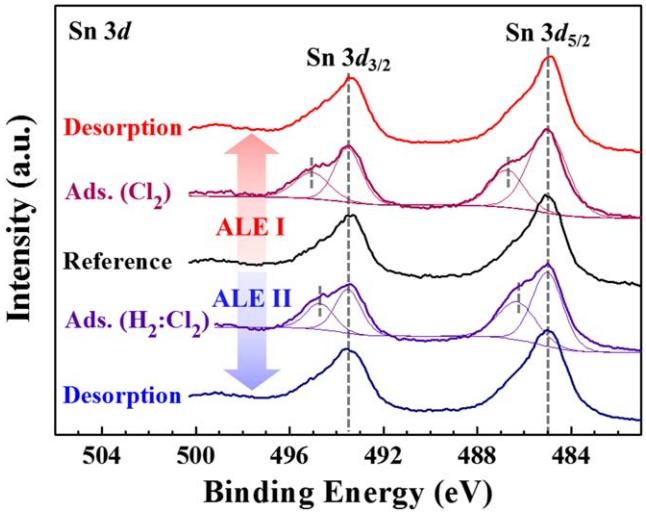

Figure 7. XPS narrow scan spectra of Sn 3*d* after the adsorption and desorption for the Sn ALEs (ALE I and ALE II in figure 4(b)).

modified layer formed on the Sn surface. When, the H_2/Cl_2 gas ratio of 1/5 was used, the EPC was saturated at the lower 1st grid voltage of +30 V to +50 V, and the further increase of 1st grid voltage from +60 V increased the EPC due to the sputtering of Sn exposed after the removal of the SnH_xCl_y. Therefore, by using the H_2/Cl_2 of 1/5 instead of pure Cl_2, the increased ion energy window for ALE could be obtained possibly due to the formation of a more volatile SnH_xCl_y compared to $SnCl_x$ on the Sn surface during the adsorption step. For the adsorption gas ratios of $H_2/Cl_2 \geqslant 1{:}3$, no saturation of EPC with the 1st grid voltage was observed due to the formation of volatile SnH_xCl_y compounds during the adsorption step. Therefore, by using the H_2/Cl_2 gas ratio of 1/5, a wider ALE window and a lower Ar^+ ion energy for the desorption step could be obtained compared to those with pure Cl_2.

To use Sn as the EUV mask absorption layer, a precise etching of Sn and a high etch selectivity over a EUV capping layer such as Ru are required. Using pure Cl_2 for adsorption and 1st grid voltage of +40 V for desorption (ALE condition I) and using the H_2/Cl_2 gas ratio of 1/5 for adsorption and 1st grid voltage of +30 V for desorption (ALE condition II), the etch depths of Sn and Ru were measured as a function of the number of etch cycles and the results are shown in figure 4(b). To minimize the Ru damage, the lowest Ar^+ ion energies for desorption was used for the ALEs. As shown in figure 4(b), the etch depths were increased linearly with etch cycles with the EPC of ~2.6 Å $cycle^{-1}$ for both ALE I and ALE II. In the case of Ru, no etching was observed until 200 cycles for both ALE I and ALE II.

For the adsorption step, H_2/Cl_2 plasmas are generated in the ICP source, therefore, the ratios of H and Cl radicals formed in the ICP source for different gas ratios of H_2/Cl_2 were investigated using OES and the results are shown in figure 5. For the comparison of H and Cl radicals, 0.3 mTorr of Ar was added in the plasmas. Figure 5(a) shows the OES spectra for different H_2/Cl_2 gas ratios and, as shown in figure 5(a), the increase of H_2 in the H_2/Cl_2 gas ratios increased the peak intensities of H_β (486 nm) and H_α (656 nm) while the increase of Cl_2 increased the peak intensities of 808 and 837 nm related to Cl. In addition, the Ar peak intensity was observed at 751 nm. The ratios of H(656 nm)/Ar(751 nm) and Cl(837 nm)/Ar(752 nm) were measured for different gas ratios of H_2/Cl_2 for the rough estimation of H and Cl radicals from the OES intensities and the results are shown in figure 5(b). The increase of Cl_2 in the H_2/Cl_2 gas mixtures increased the Cl/Ar optical emission intensity ratio. However, in the case of H/Ar ratio, it was initially higher for the H_2/Cl_2 ratios of 5/1 and 3/1 compared to H_2 only and the further increase of H_2/Cl_2 ratio decreased the H/Ar. Higher H/Ar ratios at H_2/Cl_2 ratios of 5/1 and 3/1 compared to pure H_2 might be related to the difficulty in forming pure H_2 plasma compared to H_2/Cl_2 plasmas (the ionization energies for H and H_2 are 13.6 and 15.48 eV, respectively, while those for Cl and Cl_2 are 12.97 and 11.8 eV, respectively) [25–27]. The higher H/Ar ratios in the H_2/Cl_2 gas ratios of 1/5 and 1/3 compared to that in pure H_2 are believed to be related to the higher EPCs observed for the H_2/Cl_2 gas ratios of 1/5 and 1/3 compared to that for pure H_2 in figures 3 and 4(a).

To estimate the physical damage during the Sn ALE, the changes in surface roughness of Sn and Ru during the ALE for the desorption time from 0 to 20 s were investigated with AFM for the two ALE conditions of ALE I and ALE II shown in figure 4(b) and the results are shown in figure 6. Before the etching, the RMS surface roughness of Sn was ~2.4 nm and, after the adsorption, the measured surface roughness was ~2.5 nm for ALE I and ~2.5 nm for ALE II, therefore, no significant change in surface roughness was observed after the adsorption. During the desorption, the surface roughness was initially increased to ~2.6 nm for ALE I and ~2.7 nm for ALE II due to the partial removal of the $SnCl_x$ or SnH_xCl_y formed on the Sn surface. And, the increase of desorption time to 15 s decreased the surface roughness back to ~2.5 nm for ALE I and to ~2.5 nm for ALE II by the complete removal of the $SnCl_x$ or SnH_xCl_y layer. And, the further increase of desorption time to 20 s did not change the surface roughness significantly by showing ~2.5 nm for ALE I and ~2.5 nm for ALE II. The 5 μm × 5 μm 3D AFM images of Sn surface during Sn ALE processes of ALE I and ALE II in figure 6(b) show no significant changes in surface roughness after ALEs. Therefore, the Sn ALE processes did not change the Sn surface roughness noticeably after the etching for both ALE I and ALE II even though the surface roughness for ALE II was slightly higher possibly due to the nonuniform formation of SnH_xCl_y compared to $SnCl_x$ on the Sn surface during the adsorption.

In the case of Ru, when the Ru was exposed to the Sn ALE, as shown in figure 6(b), no increase of surface roughness was observed after the adsorption step and, during the desorption step, with increasing the desorption time, the decrease of surface roughness for both ALE I and ALE II was observed with increasing desorption time from 1.31 nm (adsorption) to 0.63 nm (20 s desorption) for ALE I and from 1.32 nm (adsorption) to 0.53 nm (20 s desorption) for ALE II without etching the Ru as shown in figure 4(b). (The 3D AFM

Table 2. The surface composition of Sn in the optimized ALE adsorption and desorption conditions.

		ALE I		ALE II	
	Reference	Adsorption (Cl_2)	Desorption (Ar^+)	Adsorption (H_2/Cl_2, 1:5)	Desorption (Ar^+)
Sn	91.2	72.3	90.5	75.3	92.0
Cl	0	21.8	2.7	18.7	1.8
O	8.8	5.9	6.8	6.0	6.2

images for Ru during the ALE processes of ALE I and ALE II are shown in the supplementary figure S2) The decreased surface roughness with increasing the desorption time appears to be related to the surface smoothing effect by a low energy Ar^+ ion bombardment.

The binding states of Sn surface after the adsorption and desorption during the Sn ALEs (ALE I and ALE II in figure 4(b)) were investigated by Sn 3*d* XPS narrow scan spectra and the results are shown in figure 7. Before the etching, Sn $3d_{5/2}$ and $3d_{3/2}$ peaks were confirmed at 485.0 and 493.5 eV, respectively and, after the adsorption with Cl_2 for 15 s, the additional peaks at 486.5 and 495.0 eV related to the Sn-Cl bonding could be observed. In the case of adsorption with H_2/Cl_2 of 1/5 for 15 s, additional peaks at 486.2 and 494.7 eV which are slightly lower than those for pure Cl_2 were observed possibly due to the formation of H-Sn-Cl bonding. However, for both ALE conditions, the additional peaks were completely disappeared after the desorption for 15 s. The changes in bonding states of Ru surface during the adsorption and desorption for Sn ALE conditions were also investigated. However, during the adsorption and desorption of the Sn ALE cycles, the binding energies of the Ru surface were not affected and were remained the same as those of reference Ru for both ALE I and ALE II confirming that the Sn ALE processes do not cause any chemical damage to the Ru surface (see supplementary figure S3).

The changes in the composition of Sn surface during the Sn ALE during the adsorption and desorption of Sn ALE are shown in table 2. Before the adsorption, the surface composition of Sn was ~91.2% of Sn and ~8.8% of oxygen. After the adsorption with Cl_2 for the ALE I, the composition of Sn surface was changed to Sn:Cl:O = 72.3:21.8:5.9% and, after the adsorption with H_2/Cl_2 of 1/5 for the ALE II, it was changed to Sn:Cl:O = 75.3:18.7:6.0%, therefore, adsorption of Cl on Sn surface during the adsorption step could be identified for both ALE I and ALE II. After the desorption with Ar^+ ions for 15 s, the surface composition was changed to Sn:Cl:O = 90.5:2.7:6.8% for ALE I and to 92.0:1.8:6.2% for ALE II, therefore, most of adsorbed Cl was removed on the Sn surface after the desorption step for both ALEs. Oxygen percentages observed on the Sn surfaces before the adsorption (the reference), after adsorption, and after the desorption are believed to be related to the oxidation of Sn surface during the exposure to air. In addition, for the adsorption condition of H_2/Cl_2 (1/5) in the ALE II, the adsorption of H on the Sn surface in addition to Cl, that is, the formation of SnH_xCl_y on the Sn surface, and the complete removal of H after the desorption step could be identified by SIMS (supplementary figure S4).

4. Conclusions

Next generation EUV mask requires a thin thickness of the absorption layer with a high absorption coefficient due to the shadowing effect, and, for the formation of EUV mask, a precise etch control of the absorption layer in addition to a high etch selectivity over the capping layer is required. Using Sn as one of the next generation absorbing layers with a high absorption coefficient, the ALE techniques of Sn were investigated using H/Cl radicals as the adsorption species and energetic Ar^+ ions for the desorption. For the adsorption with H/Cl radicals with H_2/Cl_2 plasmas, it is found that, the H_2/Cl_2 gas ratios $\leqslant 1/5$ are required due to the spontaneous etching of Sn for H_2/Cl_2 gas ratios $\geqslant 1/3$. Also, for the desorption with Ar^+ ions, due to the noticeable sputtering of Sn, 1st grid voltage of $\leqslant +50$ V (Ar^+ ion beam energy ~65 eV) of the ICP ion beam source was required. The adsorption with H_2/Cl_2 of 1/5 showed a wide ALE windows of 1st grid voltage from +30 to +50 V compared to the adsorption with pure Cl_2 having the ALE window from +40 to +50 V due to the higher volatility of SnH_xCl_y compared to $SnCl_x$ formed on the surface through reaction of Sn with H_2/Cl_2 and Cl_2, respectively, even though the EPCs were the same as ~2.6 Å $cycle^{-1}$ under optimized ALE process conditions (+30 V of 1st grid voltage for H_2/Cl_2 of 1/5 and +40 V of 1st grid voltage for pure Cl_2). In the optimized ALE processes, no noticeable physical and chemical damages were observed on Sn surface. Also, when Ru, which is used as an EUV capping layer, was exposed to the Sn ALE conditions, not only no etching of Ru with the Sn ALE conditions but also no physical and chemical damages of the Ru surface could be observed. Therefore, it is believed that, by using ALE methods with a H_2/Cl_2 (1/5) gas mixture for adsorption and with a controlled Ar^+ ion energy for desorption, not only a precise atomically controlled etching of EUV mask absorbing layer but also a high etch selectivity over the capping layer could be obtained without physical and chemical damages.

Acknowledgments

This work was supported by SamSung Electronics Co., Ltd (IO201211-08086-01) and the National Research Foundation

of Korea (NRF) grant funded by the Korea government (MSIT) (2018R1A2A3074950) and the MOTIE [Ministry of Trade, Industry & Energy (20003665)] and KSRC (Korea Semiconductor Research Consortium) support program for the development of the future semiconductor device.

Data availability statement

All data that support the findings of this study are included within the article (and any supplementary files).

ORCID iDs

Doo San Kim https://orcid.org/0000-0002-5598-1358
Geun Young Yeom https://orcid.org/0000-0002-1176-7448

References

[1] Wu B and Kumar A 2007 *J. Vac. Sci. Technol.* B **25** 1743
[2] Nakamura N *et al* 2009 *Presented in Part at IEEE Int. Electron Devices Meeting (IEDM), USA*
[3] Wei A, Wallace C, Phillips M, Knudsen J, Chakravarty S, Shamanna M and Brain R 2020 *Presented in Part at IEEE Int. Electron Devices Meeting (IEDM), USA, Dec.*
[4] Buitrago E, Fallica R, Fan D, Kulmala T S, Vockenhuber M and Ekinci Y 2016 *Microelectron. Eng.* **155** 44
[5] Benschop J, Banine V, Lok S and Loopstra E 2008 *J. Vac. Sci. Technol.* B **26** 2204
[6] Belau L, Park J Y, Liang T, Seo H and Somorjai G A 2009 *J. Vac. Sci. Technol.* B **27** 1919
[7] Motai K, Oizumi H, Miyagaki S, Nishiyama I, Izumi A, Ueno T, Miyazaki Y and Namiki A 2007 *Presented in Part at SPIE Advanced Lithography, USA, Mar.*
[8] Niibe M, Watanabe T, Nii H, Tanaka T and Kinoshita H 2000 *Jpn. J. Appl. Phys.* **39** 6815
[9] Erdmann A, Mesilhy H, Evanschitzky P, Philipsen V, Timmermans F and Bauer M 2020 *J. Micro/Nanolith. Mems Moems* **19** 041001
[10] Wu M *et al Micro Nano Eng.* 2021 **12** 100089
[11] Mangat P J S *et al* 1999 *J. Vac. Sci. Technol.* B **17** 3029
[12] Luong V, Philipsen V, Hendrickx E, Opsomer K, Detavernier C, Laubis C, Scholze F and Heyns M 2018 *Appl. Sci.* **8** 521
[13] Kim T G, Kim B H, Kang I Y, Chung Y C, Ahn J, Lee S Y, Park I S, Kim C Y and Lee N E 2006 *J. Vac. Sci. Technol.* B **24** 2820
[14] Herpen M M J W, Klunder D J W, Soer W A, Moors R and Banine V 2010 *Chem. Phys. Lett.* **484** 197
[15] Wu B 2006 *J. Vac. Sci. Technol.* B **24** 1
[16] Letzkus F, Butschke J, Irmscher M, Kamm F M, Koepernik C, Mathuni J, Rau J and Ruhl G 2004 *Microelectron. Eng.* **73-74** 282
[17] Park W, Kwon O, Whang K W and Lee J 2012 *J. Vac. Sci. Technol.* A **30** 041301
[18] Wu B and Kumar A 2007 *Appl. Phys. Lett.* **90** 063105
[19] Shin M H, Na S W, Lee N E and Ahn J H 2006 *Thin Solid Films* **506-507** 230–4
[20] Park J W, Kim D S, Lee W O, Kim J E and Yeom G Y 2019 *Nanotechnology* **30** 085303
[21] Sang X, Chen E and Chang J P 2020 *J. Vac. Sci. Technol.* A **38** 042603
[22] Sang X and Chang J P 2020 *J. Vac. Sci. Technol.* A **38** 042604
[23] Elg D T, Panici G A, Peck J A, Srivastava S N and Ruzic D N 2017 *J. Micro/Nanolith. Mems Moems* **16** 023501
[24] Faradzhev N and Sidorkin V 2009 *J. Vac. Sci. Technol.* A **27** 306
[25] Lenntech (https://lenntech.com/periodic-chart-elements/ionization-energy.htm)
[26] Chemistry LibreTexts Online (https://chem.libretexts.org/Bookshelves/Physical_and_ Theoretical_Chemistry_Textbook_Maps/Supplemental_Modules_(Physical_and_Theoretical_Chemistry)/Atomic_Theory/Ionization_Energies_of_Diatomic_Molecule)
[27] Frost D C and McDowell C A 1960 *Can. J. Chem.* **38** 407